In vivo correlation mapping microscopy

James McGrath,[a] Sergey Alexandrov,[a] Peter Owens, [b] Hrebesh Subhash, [a] Martin Leahy[a, c*]
[a]National University of Ireland Galway, Tissue Optics and Microcirculation Imaging Group, National Biophotonics and Imaging Platform, Physics Department, University Rd., Newcastle, Galway, Ireland, H91 TK33
[b]Centre for Microscopy and Imaging, National University of Ireland Galway, University Rd., Newcastle, Galway, Ireland, H91 TK33
[c]RCSI Royal College of Surgeons, 123 St. Stephens Green, Dublin 2, Ireland, D02 YN77

Abstract. To facilitate regular assessment of the microcirculation in-vivo, non-invasive imaging techniques such as nailfold capillaroscopy are required in clinics. Recently a correlation mapping technique has been applied to Optical Coherence Tomography (OCT) which extends the capabilities of OCT to microcirculation morphology imaging. This technique, known as cmOCT has been shown to extract parameters such as capillary density and vessel diameter, key clinical markers associated with early changes in microvascular diseases. However, OCT has limited spatial resolution in both the transverse and depth directions. Here, we extend this correlation mapping technique to other microscopy modalities, including confocal microscopy and take advantage of the higher spatial resolution offered by these modalities. The technique is achieved as a processing step on microscopy images and does not require any modification to the microscope hardware. Results are presented which show that this correlation mapping microscopy technique can extend the capabilities of conventional microscopy to enable mapping of vascular networks in-vivo with high spatial resolution in both the transverse and depth directions.

Keywords: confocal microscopy, wide field microscopy, nailfold capillaroscopy, biomedical optical imaging, correlation mapping.

***Martin Leahy, E-mail: martin.leahy@nuigalway.ie

1 Introduction

The microcirculation is the term used to describe the small blood vessels (< 100 μm in size) in the vasculature network which are vital for tissue nutrition and shape as well as waste removal, blood pressure and temperature regulation, and oxygen supply. Structural and functional changes in the microcirculation are associated with various pathological conditions including diabetes, Raynaud's disease, psoriasis, systemic sclerosis and hypertension.[1] A frequently used modality for non-invasive examination of the microcirculation is laser Doppler blood perfusion monitoring, which is based on measuring the Doppler shift induced by moving red blood cells.[2] Laser Doppler uses diffuse light from the top approximately 1 mm of tissue to provide average perfusion measurements over volumes of approximately 100 μm^3 and is unable to provide information on individual smaller vessels.

Video capillaroscopy[3], an extension of bright wide field microscopy is a simple and cost-effective modality for assessment of the microcirculation and is used in the diagnosis and follow up of many pathological conditions. However, it is generally limited in application to sites such as nailfold plexus and conjunctiva where the blood vessels are close to the surface so that they are not obscured by scattering. Sidestream dark field imaging can extend these techniques for application to other cardiovascular diseases by improved imaging of the tongue and oral mucosa.[4,5] More recently, reflectance-mode confocal microscopy has also been introduced to assess the human skin microcirculation.[6,7,8] Optical coherence tomography (OCT) is an emerging noninvasive imaging technique which can generate depth resolved images of the microcirculation[9,10,11]. However OCT itself does not directly produce these images of microcirculation. Several technologies have been developed to extend the capabilities of OCT to visualize the microcirculation such as Doppler OCT[12].

Figure 1 shows a plot of the typical resolution vs. sampling depth for the widefield microscopy, confocal microscopy and OCT modalities. OCT has the advantage of imaging 1-2 mm in tissue (typically 1 mm in human skin), but with limited spatial resolution, typically on the order of 10 - 20 μm. The higher lateral resolution of widefield and confocal microscopy modalities makes them very suitable for imaging of the smaller cutaneous vessels non-invasively, in real time, and with a resolution comparable to that of histological examination. Longer wavelengths, e.g. 830 nm have improved the imaging depth in skin up to 300 μm in some cases.[6] Widefield and confocal microscopy can potentially therefore be used to complement OCT imaging as they can provide information on the smaller capillaries in the dermal-epidermal junction whereas OCT can provide information on larger vessels deeper in the skin.

A correlation mapping algorithm has been previously developed and applied by our group to Optical Coherence Tomography (OCT).[9,10,11] The technique, known as correlation mapping OCT (cmOCT) utilizes the time-varying speckle effect. This effect, produced by moving scatters, provides contrast between regions of flow and static tissue, facilitating the generation of maps of microcirculation morphology. Recently a similar correlation mapping algorithm has been implemented in real time by utilizing graphics processing units (GPU's).[13]

In this work, we extend the correlation mapping technique to wide field and confocal microscopy. Correlation mapping microscopy enables wide field and confocal microscopy to visualize flow, for example the microcirculation, with a high contrast, and takes advantage of the higher spatial resolution afforded by these modalities. This technique utilizes the light intensity variations over time caused by moving scatterers to provide contrast against a static background. Flow visualization is achieved by correlating temporally consecutive microscopy image frames to extract the flow information and does not require any modification or addition to the microscope hardware.[14] The adaptation of the correlation mapping algorithm to microscopy images is demonstrated, including visualization of a capillary tube flow phantom through a scattering medium, and in-vivo human imaging of the volar forearm.

2 Processing principles of correlation mapping microscopy

2.1 Correlation mapping microscopy processing technique

The correlation mapping algorithm is applied to consecutive pairs of microscopy images. The first step of the algorithm is to suppress noise, which will cause decorrelation, by applying a "structural mask" to the images. The structural mask includes regions that contain structural information in the microscopy image. The mask is generated by performing a kernel average

followed by a binary threshold on the source microscopy images. A kernel is a 2D array of image pixels, the size of which is determined by the user.

The next step is determination of the correlation between two temporally consecutive microscopy images captured at the same location. This is calculated by using a Pearson correlation to cross correlate a grid from microscope image A (I_A) to the same grid from image B (I_B):

$$\boldsymbol{cm}(\boldsymbol{x},\boldsymbol{y}) = \sum_{\boldsymbol{p=0}}^{\boldsymbol{M}} \sum_{\boldsymbol{q=0}}^{\boldsymbol{N}} \frac{\left[\boldsymbol{I_A}(\boldsymbol{x+p},\boldsymbol{y+q}) - \boldsymbol{I'_A}(\boldsymbol{x},\boldsymbol{y})\right]\left[\boldsymbol{I_B}(\boldsymbol{x+p},\boldsymbol{y+q}) - \boldsymbol{I'_B}(\boldsymbol{x},\boldsymbol{y})\right]}{\sqrt{\left[\boldsymbol{I_A}(\boldsymbol{x+p},\boldsymbol{y+q}) - \boldsymbol{I'_A}(\boldsymbol{x},\boldsymbol{y})\right]^{\boldsymbol{2}}\left[\boldsymbol{I_B}(\boldsymbol{x+p},\boldsymbol{y+q}) - \boldsymbol{I'_B}(\boldsymbol{x},\boldsymbol{y})\right]^{\boldsymbol{2}}}} \quad \text{(Eq. 1)}$$

Equation 1 is the Pearson correlation formula and is a measure of the linear correlation between two variables, giving a value between +1 and -1 inclusive. According to this equation, a value of +1 represents total positive correlation and a value of -1 represents total negative correlation. We would expect static features to have correlation values of close to +1, while regions of flow will have much lower correlation values.

The grids I_A and I_B are stepped across the whole image, and a correlation value is calculated at each pixel resulting in a two-dimensional correlation map. The resultant map has correlation values in the range 0 ± 1. This allows for immediate determination of flow regions as higher correlation represents static regions of the sample and lower correlation values represents regions of flow within the sample. Noise present in the images generated by the system could lower the correlation value of static features, as noise would cause decorrelation. In our image processing we assume correlation values of >0.6 are static features.

In the phantom studies, the ability of the correlation mapping algorithm to contrast the flow region is validated using the correlation signal to noise ratio. Metrics such as the correlation signal to noise ratio have previously been used to evaluate the quality of angiography algorithms[15]. Correlation signal to noise ratio (CSNR) is defined as:

$$CSNR = \frac{\overline{C_{flow}} - \overline{C_{static}}}{\sqrt{\sigma^2_{static}}} \quad \text{(Eq. 2)}$$

$\overline{C_{flow}}$ and $\overline{C_{static}}$ are the average correlation values in flow and static regions respectively and σ^2_{static} is the variance of the correlation within static region. CSNR values are calculated in each of the following studies to illustrate the ability of the correlation mapping algorithm to contrast flow and static regions.

The optimal kernel size must be selected by the user. The kernel size used in this work was arbitrarily chosen for optimal image quality with the trade-off of processing time, spatial resolution and CSNR. Larger kernels require greater processing times but are less susceptible to noise than smaller size kernels. However, very large kernel sizes causing "blurring" in the correlation map image, which will make smaller regions of flow undetectable from an in vivo perspective. From an in-vivo perspective. If the aim is to detect smaller capillaries or if the aim is to measure capillary diameter this will be a significant issue. If a very small kernel is used such as 3 x 3, the resulting data set can be quite noisy as small changes in the structural signal can result in decorrelation and may be mistaken for regions of flow. An optimum kernel size must be determined. In this work a kernel size of 11 x 11 was used as it delivered a good quality image with an acceptable signal to noise ratio while providing sufficient spatial resolution to avoid incurring any image blurring which larger kernel sizes would cause.

Implementation of the correlation mapping microscopy algorithm is an 'in-house' developed multi-threaded code written using the Java programming language. The program can process 30 adjacent microscopy images of size 1000 by 1000 pixels in < 1.5 seconds using 8 threads. Further speed up could be achieved using optimized code or GPU based techniques, enabling implementation of the algorithm in real time.

The dynamic range of velocity depends on a variety of factors, including frame rate and resolution. There must be enough time between frames so that the movement of the particles in the liquid can be detected within a given resolution. Confocal microscopy has better resolution and because of this should be able to operate at higher frame rate and give the best dynamic range of velocities.

2.2 Wide field/confocal microscopes and OCT system

To validate the correlation mapping microscopy algorithm a variety of microscope systems were used in this study. The wide field microscope used was an Olympus Measuring Microscope (STM-MJS2), using a broadband white light source with an Olympus MS Plan 10x objective lens with a numerical aperture of 0.3, giving the system a lateral resolution of 1.1 μm. Images were captured using a Lumenera Infinity 2 digital CCD camera operating at ~1 frame per second (fps).

Reflectance confocal microscopy images were acquired with an Andor Revolution Spinning Disk (Andor Technology Ltd., Belfast, UK) system operating at a wavelength of 640 nm and capturing images at 15 fps. Using a 10x objective lens of *NA* 0.3 the lateral resolution of this system was 0.85 μm and the axial resolution was 9.31 μm.

In-vivo images were acquired using a reflectance confocal microscope, Vivascope 1500® (Lucid Inc, Rochester, NY, USA), a commercial clinical research system using an 830 nm (near-infrared) laser. This operating wavelength of 830 nm is at an "optical window" of the skin (mean free path for scattering ~100 μm) and thus the system facilitates investigation of the epidermis and papillary dermis to a depth of ~350 μm with a lateral resolution of 0.4 μm and an axial resolution of 1.9 μm in the center of the image field. The laser power is relatively low at 30 mW,

therefore avoiding any tissue damage. An imaging frame rate of 9 fps is achievable with a field of view of 1000 x 1000 μm.

For evaluation of in-vivo correlation mapping microscopy images, a comparison was performed with images taken from a commercial OCT system (OCM1300SS, Thorlabs Inc., Newton, NJ, USA). This is a Fourier-domain system using a swept source laser (SL1325-P16 Thorlabs Inc.) operating at a center wavelength of 1325 nm and at a scanning rate of 16 kHz providing an axial resolution of ~12 μm and a lateral resolution of 25 μm.

3 Phantom imaging

3.1 Wide field microscopy phantom imaging

To demonstrate the ability of correlation mapping microscopy to extract flow with low velocities, a capillary tube sample was fabricated. The sample consisted of a glass capillary tube, mounted on a piece of black card and filled with 3% intralipid solution which was free to move under Brownian motion. This tube appears on the right hand side in Fig. 2 parts (a) and (b). A separate empty glass capillary tube was also mounted on the black card. This tube appears on the left hand side in Fig. 2 parts (a) and (b). Both capillary tubes had an internal diameter of 100 μm. The wide field microscope focus was set to the center of the capillary tubes and a series of images were taken as shown in Fig. 2 parts (a) and (b). Movie clips are provided for Fig. 2 parts (a) and (b). It is very difficult to differentiate any flow/Brownian motion regions from static regions by examining these images and movie. The correlation map resulting from applying the correlation mapping microscopy algorithm to these two temporally consecutive images is shown in Fig. 2 part (c). A movie is also provided for part Fig. 2 part (c). In this image and in the corresponding movie it can be seen that the capillary tube on the right hand side containing the

intralipid solution moving under Brownian motion is highlighted by brighter colors representing lower correlation values. To calculate the CSNR value, a region of interest in both a static area and an area of flow/Brownian motion needed to be analyzed. A 50 x 50 pixel region within both the empty capillary tube (Blue Square on Fig. 2 part (c) and capillary tube filled with intralipid (green square on Fig. 2 part (c)) was selected. The resulting CSNR value was 10.89. This illustrates the ability of the correlation mapping microscopy algorithm to clearly visualize the region of flow within the image.

3.2 Wide field microscopy phantom imaging through scattering medium

The aim of the next experiment was to test the ability of correlation mapping microscopy to detect flow when imaging through a scattering medium. To test this, the sample used in Sec. 3.1 was covered with a layer of semi-transparent scotch tape from the 3M company. This tape has a mean thickness of 60 μm and a scattering angle of about 5 degrees. The wide field microscope was focused to the center of the capillary tubes and a series of images was taken, an example of which is shown in Fig. 3 part (a). A movie is provided corresponding to Fig. 3 parts (a) and (b). The capillary tube in the upper part of Fig. 3 part (a) contains 3% intralipid solution moving under Brownian motion, the lower capillary tube is empty. Fig. 3 part (b) clearly shows the upper capillary tube containing the intralipid solution highlighted by brighter colors representing lower correlation values. To calculate the CSNR value, a region of interest in both a static area and an area of flow/Brownian motion needed to be analyzed. A 50 x 50 pixel region within both the empty capillary tube (Blue Square on Fig. 3 part (b) and capillary tube filled with intralipid (green square on Fig. 3 part (b)) was selected. The resulting CSNR value was 5.12. This illustrates the ability of the correlation mapping microscopy algorithm to clearly visualize the region of flow within the image, even when imaging through a scattering medium.

3.3 Confocal microscopy phantom imaging

We next tested the applicability of the correlation mapping microscopy algorithm to confocal microscopy. A capillary tube sample containing three tubes filled with 3% intralipid solution was prepared. The three tubes, with inner diameters 50 μm, 100 μm and 200 μm were mounted on a glass microscope slide as shown in Fig. 3 part (a). Imaging was performed with the Andor Revolution spinning disk confocal microscope described in Sec. 2.1 with the imaging depth set to approximately the center of the 50 μm inner diameter capillary tube. A movie is provided corresponding to Fig. 4 parts (a) and (b). From the conventional microscopy images it is very difficult to differentiate static regions from regions of flow. The correlation mapping microscopy algorithm, described in 2.1, was applied to two temporally consecutive confocal microscope images of the sample. The resulting correlation map is shown in Fig. 4 part (b). Once again, the internal cavity of the capillary tubes is highlighted in brighter colors corresponding to low correlation values, differentiating these regions as containing flow/liquid moving under Brownian motion as opposed to the darker colored static regions between the tubes. To calculate the CSNR value, a region of interest in both a static area and an area of flow/Brownian motion needed to be analyzed. A 50 x 50 pixel region within the 50 μm capillary tube containing intralipid was selected to represent a region of Brownian motion (Green Square on Fig. 4 part (b). Additionally a 50 x 50 pixel region between the 50 μm and 100 μm capillary tubes was selected to represent a static region (Blue Square on Fig. 4 part (b). The resulting CSNR value was 6.30. This result demonstrate possibility of the correlation mapping confocal microscopy clearly visualize regions with flow.

3.4 In-vivo imaging

To demonstrate the clinical suitability of correlation mapping microscopy and compare it to established microcirculation imaging modalities, in-vivo imaging was performed. Both in-vivo confocal microscopy using the Vivascope 1500 and OCT using the Thorlabs systems described in Sec. 2.1 was performed on the volar forearm of a 27 year old male with informed consent. The OCT image together with its derived cmOCT image of the volar forearm at a depth of ~250 μm is shown in Fig. 5 parts (a) and (b) respectively. These images have a field of view of 3000 μm x 3000 μm. A zoomed in portion of the OCT image is shown in Fig. 5 part (d) and of the cmOCT image in Fig. 5 part (e). These images have a field of view of 500 μm x 500 μm, the same as that of images generated by the Vivascope 1500 reflectance confocal microscopy system. It is difficult to make out vessel structure and location from low resolution OCT and cmOCT images in Fig. 5 parts (a-e).

An example image of the volar forearm generated by the Vivascope 1500 confocal microcopy system is shown in Fig. 5 part (f). The dermal papillae are visible in the confocal microscopy image of Fig. 5 part (f) as bright circular basal layers with a dark center. Inside these circles, the lumina of the capillary loops are apparent as black holes and appear in pairs, with an arterial and a venous capillary located next to one another. After applying the correlation mapping algorithm to these images, the microcirculation is clearly visualized with high contrast (as shown in Fig. 5 part (g)), allowing us to investigate vessels of size 10-20 μm located in the dermal-epidermal junction layer. The correlation maps can be averaged across a number of frames (5 in this case) to give a clearer image. This averaging could be reduced or eliminated if sample motion is reduced either with improved mounts or motion correction image processing algorithms. Averaging is not performed on the OCT data, however a motion compensation algorithm is

applied to reduce any effect of axial or lateral motion. It is impossible to visualize vessels in the dermal papillae using most currently available commercial OCT systems. The observed locations of vessels in Fig. 5 part (g) match well with the locations of vessels you would expect from an examination of Fig. 5 part (f). Note that while the dermal papillae are easy to identify in the confocal reflectance microscopy image of Fig. 5 part (f), not all of these structures contain currently dilated vessels with blood flow. After application of the correlation mapping algorithm the regions of blood flow are easily identified. To calculate the CSNR value, a region of interest in both a static area and an area of flow/Brownian motion needed to be analyzed. A static region was identified as a region of tissue outside the dermal papillae, where no blood vessels are present (Blue square in Fig. 5 part (g)). Within the dermal papillae, blood vessels are present and a region in this area was chosen as the 'flow' region. This is identifiable as the region within the green square in Fig. 5 part (g). A 50 x 50 pixel area of both these static and flow regions was selected and the CSNR was calculated. The resulting CSNR value was 4.95.

It is noted that it is possible to calculate additional information, such as capillary loop density and vessel diameter from Fig. 5 part (g). Calculation of these markers was performed by first loading the in-vivo confocal images into ImageJ, which is a public domain image processing tool (version 1.49, available at http://imagej.nih.gov/ij/). The ImageJ software was calibrated with the known pixel-distance relationship. The area within the field of view of the image could then be estimated. The capillary loop density can be calculated by manually identifying and counting the number of detected vessels within this area. The capillary density of the volar forearm has been calculated to be ~28 loops/mm^2, this value is within the 14 to 30 loops/mm^2 range previously reported[16]. Additionally, the average capillary loop diameter can be estimated. Capillary size measurements between two reference points were performed by tracing a

horizontal line between clearly distinguishable inner borders of capillaries. The ImageJ software calculated the intracapillary distance in micrometers according to the previous calibration. We estimate the average capillary loop diameter to be ~9.50 µm, which is close to the value reported in previous studies[6]. Such parameters are relatively easy to determine from correlation mapping images as the patent capillaries are immediately identified. Capillaries in the dermal papillae have diameters which are below the resolution of typical commercially available OCT systems and therefore cannot be detected by such systems. Correlation mapping confocal microscopy can complement OCT in scenarios requiring imaging of small blood vessels in the dermal-epidermal junction.

4 Summary

This work has demonstrated the application of the correlation mapping algorithm to wide field and confocal microscopy modalities, including in-vivo confocal microscopy. The application of this algorithm to microscopy modalities allows identification of regions of fluid flow with high spatial resolution. Such regions of flow can be very difficult to distinguish in the raw microscopy images and movies. However we showed that after application of the correlation mapping algorithm regions of fluid flow can easily be differentiated from static regions with high contrast even when imaging through scattering media. For the flow phantoms, just two temporally consecutive microscope image frames are required to visualize flow. *In-vivo* human imaging of the volar forearm using a clinical reflectance confocal microscopy system and the correlation mapping algorithm demonstrated high resolution visualization of blood vessels which are below the resolution of the typical commercial systems of other modalities such as OCT and laser Doppler flowmetry. With correlation mapping we can clearly visualize flow areas and dynamics could potentially be estimated. These results suggest the correlation mapping microscopy an

excellent choice for imaging of different dynamic events with high resolution, for example, visualization of blood flow in small size vessels using in-vivo confocal microscopy. The correlation mapping algorithm does not require additional hardware modifications to the microscope system, is implemented entirely in software and real-time processing of microscope images can be achieved.

Acknowledgments

This work was supported by the National Biophotonics Imaging Platform (NBIP) Ireland funded under the Higher Education Authority PRTLI Cycle 4, co-funded by the Irish Government and the European Union – Investing in your future. The authors would like to the Prof. Steven Jacques of Oregon Health and Science University and National Center for Laser Applications, NUI Galway for the use of their wide field microscope. The study was approved by the Research Ethics Committee of NUI Galway.

References

1. M. J. Leahy, Ed., Microcirculation Imaging, p. 37, Wiley-VCH, Weinheim, Germany (2012) [doi:10.1002/9783527651238].
2. S. M. Daly and M. J. Leahy, "'Go with the flow': A review of methods and advancements in blood flow imaging," *J. Biophotonics.* **6**(3), 217-255, (2013) [doi:10.1002/jbio.201200071].
3. F. Gallucci, R. Russo, R. Buono, R. Acampora, E. Madrid and G. Uomo, "Indications and results of videocapillaroscopy in clinical practice," *Advances in Medical Sciences*, **53**(2), 149–157, (2008) [doi:10.2478/v10039-008-0038-4].
4. Goedhart, P.T., Khalilzada, M., Bezemer, R., Merza, J., Ince, C., "Sidestream Dark Field (SDF) imaging: a novel stroboscopic LED ring-based imaging modality for clinical assessment of the microcirculation.", *Optics Express*, **15**(23), 15101-14 (2007) [doi:10.1364/OE.15.015101]

5. Ince, C., "Sidestream dark field imaging: an improved technique to observe sublingual microcirculation.", *Crit Care*. **9**(Suppl 1), P72 (2005) [doi:10.1186/cc3135]
6. M. A. Altintas, A. A. Altintas, M. Guggenheim, A. E. Steiert, M. C. Aust, A. D. Niederbichler, C. Herold and P. M. Vogt, "Insight in human skin microcirculation using in vivo reflectance mode confocal laser scanning microscopy", *J. Digital Imaging*, **23**(4), 475-481 (2010) [doi:10.1007/s10278-009-9219-3].
7. E. Cinotti, L. Gergel, J. L. Perrot, A. Domin, B. Labeille, P. Borelli, and F. Cambazard "Quantification of capillary blood cell flow using reflectance confocal microscopy," *Skin research and technology*, **20**(3), 373–378 (2014) [doi:10.1111/srt.12128].
8. M. Venturini, M. Arisi, A. Zanca, I. Cavazzana, S. Gonzlez, F. Franceschini and P. Calzavara-Pinton, "In vivo reflectance confocal microscopy features of cutaneous microcirculation and epidermal and dermal changes in diffuse systemic sclerosis and correlation with histological and videocapillaroscopic findings," *European journal of dermatology: EJD*, **24**(3), 349–355 (2014) [doi:10.1684/ejd.2014.2321].
9. J. Enfield, E. Jonathan, and M. J. Leahy, M., "In vivo imaging of the microcirculation of the volar forearm using correlation mapping optical coherence tomography (cmOCT)," *Biomedical Optics Express*, **2**(5), 1184–1193 (2011) [doi:10.1364/BOE.2.001184].
10. E. Jonathan, J. Enfield, and M. J. Leahy, "Correlation mapping method for generating microcirculation morphology from optical coherence tomography (OCT) intensity images," *Journal of Biophotonics*, **4**(9), 583–587 (2011) [doi:10.1002/jbio.201000103]
11. A. Zam, R. Dsouza, H. M. Subhash, M. L. O'Connell, J. Enfield, K. Larin and M. J. Leahy, "Feasibility of correlation mapping optical coherence tomography (cmOCT) for anti-spoof sub-surface fingerprinting," *Journal of Biophotonics*, **6**(9), 663–667 (2013) [doi:10.1002/jbio.201200231].
12. X. Wang, T. Milner, J. Nelson, "Characterization of fluid flow velocity by optical Doppler tomography," Opt. Letters, **20**(11), 1337–1339 (1995) [doi:10.1364/OL.20.001337]

13. Y. Watanabe, H. Numazawa, and D. Kamiyama, “GPU accelerated correlation mapping OCT for real-time imaging of microvasculature,” in 2013 *Conference on Lasers and Electro-Optics Pacific Rim (CLEO-PR)*, 1–2 (June 2013) [doi:10.1109/CLEOPR.2013.6600631].
14. James McGrath ; Sergey Alexandrov ; Peter Owens ; Hrebesh M. Subhash and Martin J. Leahy, "Correlation mapping microscopy," Proc. SPIE 9322, *Dynamics and Fluctuations in Biomedical Photonics XII*, 93220L (2015) [doi:10.1117/12.2077988]
15. S. Gao, G. Liu, D. Huang and Y. Jia, “Optimization of the split-spectrum amplitude-decorrelation angiography algorithm on a spectral optical coherence tomography system”, Optics Letters, **40**(10), 2305-2308 (2015) [doi:10.1364/OL.40.002305]
16. P. Agache, P. Humbert, and H. Maibach, Measuring the Skin, p. 439, Springer-Verlag Berlin Heidelberg, Germany (2004).
17. W. S. Rasband, “ImageJ,” U. S. National Institutes of Health, Bethesda, Maryland, http://imagej.nih.gov/ij/ (1997–2015).

Figures

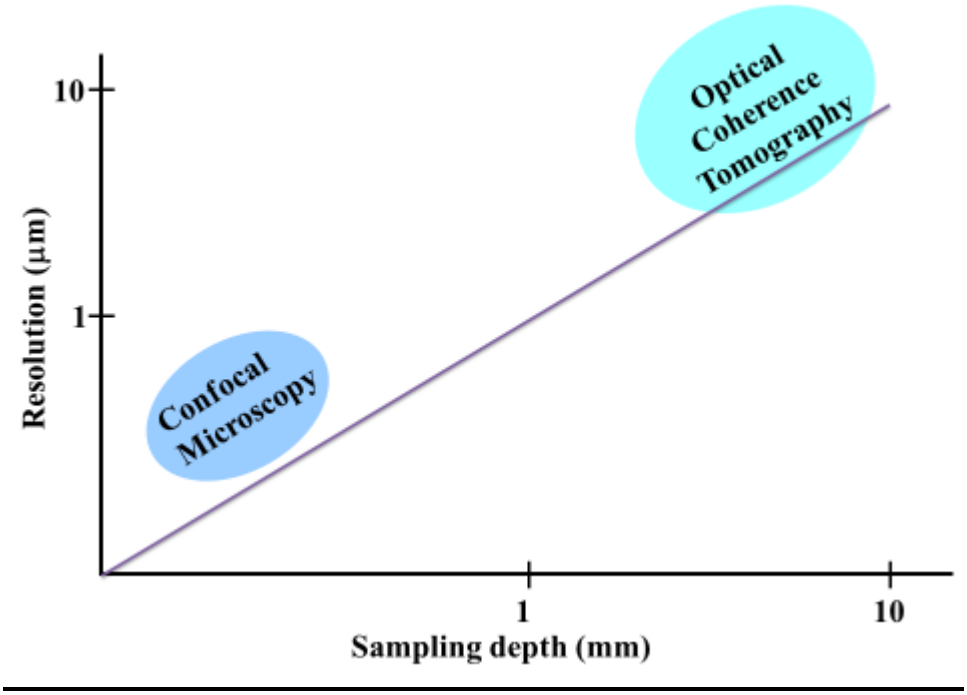

Fig. 1 Plot of resolution vs maximum sampling depth for confocal microscopy, widefield microscopy and optical coherence tomography imaging modalities.

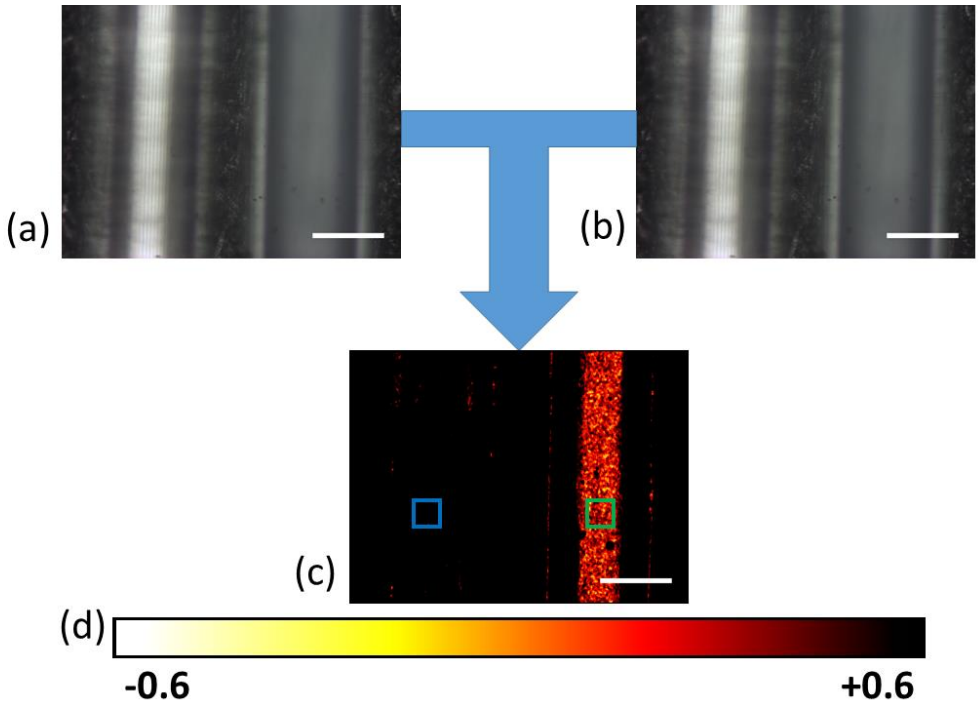

Fig. 2 Correlation mapping microscopy applied to two temporally consecutive wide field microscopy images (a) and (b). Each image shows two 100 µm inner diameter capillary tubes. In both images the tube on the left is empty and the tube on the right contains intralipid solution moving under Brownian motion. The resulting correlation map is shown in (c) with higher correlation values shown as a darker color and lower correlation values as a brighter color. CSNR was calculated between the flow region within the green square and the static region within the blue square. The scale bar in parts (a)-(c) is 100 µm. The correlation map color scale is shown in (d). A movie corresponding to (a) - (c) is provided.

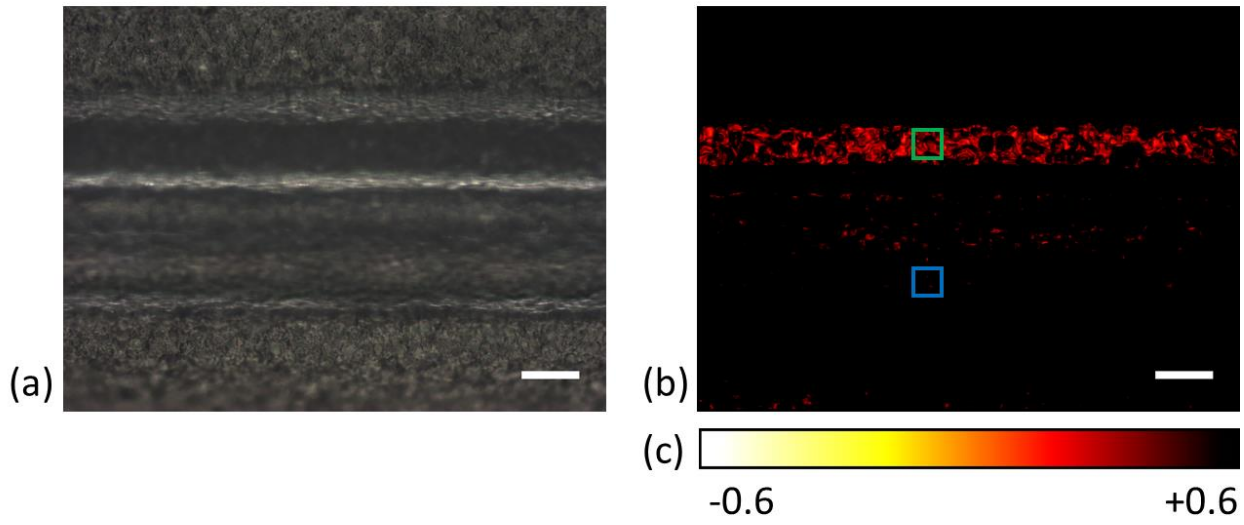

Fig. 3 Correlation mapping microscopy applied to temporally consecutive wide field microscopy images of a capillary tube sample covered with scattering sticky tape. Part (a) shows a conventional microscope image of two 100 µm inner diameter capillary tubes, the tube on the bottom is empty and the tube on the top contains intralipid solution moving under Brownian motion. The resulting correlation map is shown in (b). CSNR was calculated between the flow region within the green square and the static region within the blue square. The scale bar is 100 µm. The correlation map color scale is shown in (c). A movie corresponding to parts (a) and (b) is provided.

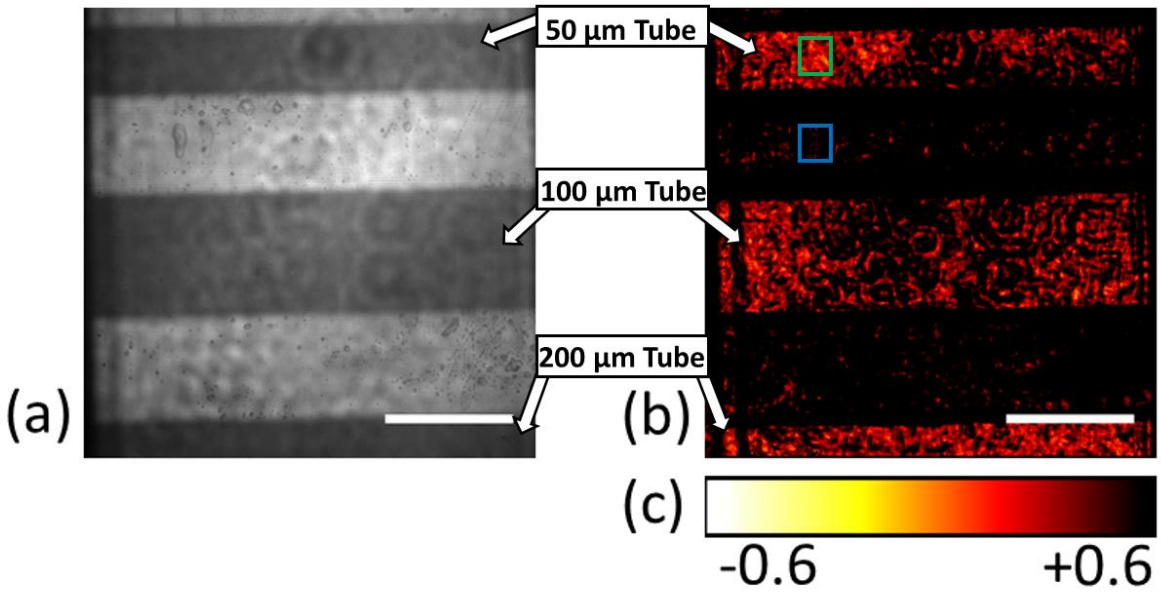

Fig. 4 Correlation mapping microscopy applied to temporally consecutive confocal microscopy images of a sample with capillary tubes of three sizes (inner diameter of 50 µm at the top, 100 µm in center and 200 µm, the upper portion of which is visible at the bottom). Conventional confocal microscope image is shown in part (a). The resulting correlation map is shown in (b). CSNR was calculated between the flow region within the green square and the static region within the blue square. The scale bar is 100 µm. The correlation map color scale is shown in (c). A movie is provided corresponding to (a) and (b).

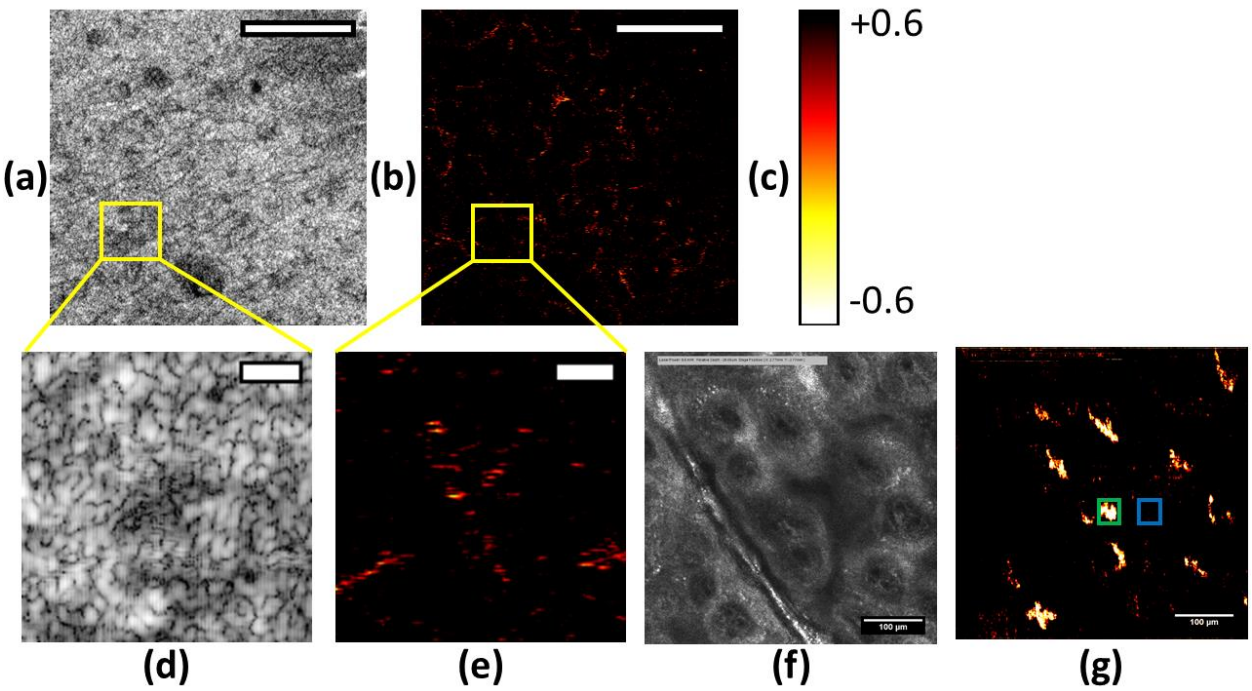

Fig. 5 In-vivo correlation mapping microscopy compared to OCT. An OCT image of the volar forearm at depth ~250 µm is shown in (a) with a cmOCT image derived from this shown in (b). Part (d) shows a zoomed in region of (a) of size 500 x 500 µm, the same dimensions of images provided by Vivascope 1500. Part (e) shows cmOCT image related to part (d). An image of the volar forearm at depth ~250 µm provided by the Vivascope is shown in (f). Part (g) shows the correlation mapping microscopy image corresponding to (f). CSNR was calculated between the flow region within the green square and the static region within the blue square in (g). Scale bars in parts (a) and (b) are 1000 µm. Scale bars in parts (d) to (g) are 100 µm. Correlation scale bar is shown in part (c).

Video Captions

Video 1 Example of a wide field microscopy image of phantom capillary tube sample (MOV, 99 KB).

Video 2 Correlation mapping microscopy movie generated from wide field microscopy frames of a capillary tube flow phantom, as in Video 1 (MOV, 530 KB).

Video 3 Example of a wide field microscopy image of phantom capillary tube sample when imaging through scattering medium (MOV, 164 KB).

Video 4 Correlation mapping microscopy movie generated from wide field microscopy frames of a capillary tube flow phantom imaged through a scattering medium, as in Video 3 (MOV, 296 KB).

Video 5 Example of a confocal microscopy image of phantom capillary tube sample (MOV, 4.6 MB).

Video 6 Correlation mapping microscopy movie generated from confocal microscopy frames of a capillary tube flow phantom, as in Video 5 (MOV, 4.6 MB).

Video 7 In vivo confocal microscopy of volar forearm (MOV, 2.5 MB).

Video 8 In vivo correlation mapping microscopy movie generated from confocal microscopy frames of volar forearm, as in Video 7 (MOV, 0.1 MB)